
Rotation-Equivariant Conditional Spherical Neural Fields for Learning a Natural Illumination Prior

James A. D. Gardner

Department of Computer Science
University of York
York, United Kingdom
james.gardner@york.ac.uk

Bernhard Egger

Cognitive Computer Vision Lab
Friedrich-Alexander-Universität
Erlangen, Germany
bernhard.egger@fau.de

William A. P. Smith

Department of Computer Science
University of York
York, United Kingdom
william.smith@york.ac.uk

Abstract

Inverse rendering is an ill-posed problem. Previous work has sought to resolve this by focussing on priors for object or scene shape or appearance. In this work, we instead focus on a prior for natural illuminations. Current methods rely on spherical harmonic lighting or other generic representations and, at best, a simplistic prior on the parameters. We propose a conditional neural field representation based on a variational auto-decoder with a SIREN network and, extending Vector Neurons, build equivariance directly into the network. Using this, we develop a rotation-equivariant, high dynamic range (HDR) neural illumination model that is compact and able to express complex, high-frequency features of natural environment maps. Training our model on a curated dataset of 1.6K HDR environment maps of natural scenes, we compare it against traditional representations, demonstrate its applicability for an inverse rendering task and show environment map completion from partial observations. A PyTorch implementation, our dataset and trained models can be found at jadgardner.github.io/RENI.

1 Introduction

Compact but expressive lighting representations play an essential role in graphics, enabling realistic lighting effects at real-time frame rates [38, 53, 54, 34, 22] and in computer vision enabling scene relighting [59, 58], face relighting [55, 43, 17, 42] and object insertion [56, 47, 31]. Real-world illumination is highly complex and variable, with a very high dynamic range, and is therefore inherently challenging to represent. However, real-world illumination does contain statistical regularities [16], particularly for outdoor, naturally lit scenes. For example, lighting usually comes predominantly from above, often with the strongest illumination coming from primary light sources in a few directions. Also, the sky and sunlight produce only a limited range of colours. In addition, illumination environments have a canonical up direction (vertical axis aligns with gravity) but arbitrary horizontal rotation (any rotation about the vertical is equally likely). These regularities and geometric symmetries can significantly restrict the space of possible illuminations to constrain inverse problems or enable the synthesis of realistic lighting.

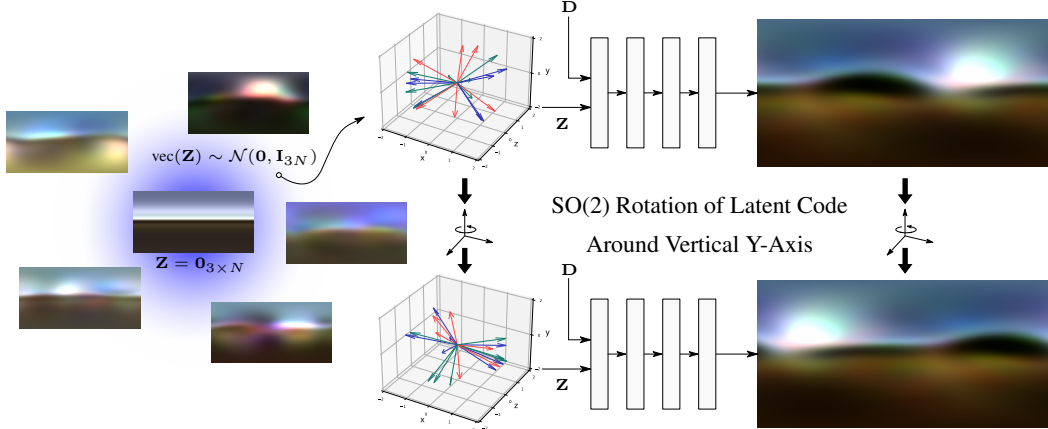


Figure 1: On the left, we visualize environment maps derived from random latent samples of RENI, our natural illumination prior, as well as the average illumination in the centre. RENI is rotation-equivariant to rotations of the latent codes around the vertical y -axis (right). Plots are shown for a 3×20 latent code at two rotations, 160 degrees apart, and the resulting output of the RENI network equally rotated.

Lighting Representations An illumination environment is a spherical signal. A relatively small set of alternatives are used for their representation within vision and graphics. A widely used representation in graphics is an environment map [39, 38, 53, 54], which is a regularly sampled 2D image representing a flattening of the sphere, usually via an equirectangular projection. However, the projection introduces distortions leading to irregular sampling on the sphere, it is not compact, introduces boundaries and provides no constraint. Nevertheless, environment map representations have been used in inverse settings where every pixel in the map is optimised independently [41].

Spherical harmonic (SH) lighting [3, 38] is a compact lighting representation commonly used in real-time computer graphics [38, 22, 46] and inverse rendering [59, 53, 31, 40, 17]. While SHs can be used to represent the illumination environment directly, more commonly, they represent pre-integrated lighting, i.e. the illumination environment convolved with a bidirectional reflectance distribution function (BRDF). When the BRDF is low frequency, as it is for Lambertian diffuse reflectance, then the convolution is also low frequency making the approximation with SHs very accurate [3].

An alternative, growing in popularity, is the Spherical Gaussian (SG) representation [54, 53, 61]. SGs represent a lighting environment as a collection of Gaussian lobes on the sphere, each of which has 6 degrees of freedom (three for RGB amplitude, two for spherical direction and one for sharpness). While this allows the reconstruction of localised high-frequency features, it still requires many lobes to approximate complex illumination environments. [31] compares SH and SG for object re-lighting, finding SG was able to recover higher frequency lighting using a similar number of parameters as SH, though both still required a large number of parameters to approximate ground truth.

Both SHs and SGs are *rotation equivariant*. A rotation of the illumination environment corresponds directly to a rotation of the SH basis or the SG lobe directions. Equivalently, they can represent any rotation of a given environment with equal accuracy. However, they provide no prior over the space of possible illuminations. SGs or SHs can represent any colour of light coming from any direction.

Illumination Priors When humans solve inverse rendering tasks, they rely on strong priors over the space of possible illuminations. For example, they resolve convex/concave shading ambiguities with the lighting-from-above assumption [26, 52]. Given this, it is surprising that statistical illumination priors have been almost completely ignored in computer vision, with the vast majority of inverse rendering techniques allowing arbitrary illumination within their chosen representation space.

There are a small number of exceptions. Both Egger et al. [17] and Yu and Smith [59] learn a linear statistical model with Gaussian prior in the space of SH coefficients. While providing a useful constraint to avoid unrealistic illumination environments, this approach inherits the weakness of SHs in being unable to reproduce high-frequency lighting effects while also losing the rotation

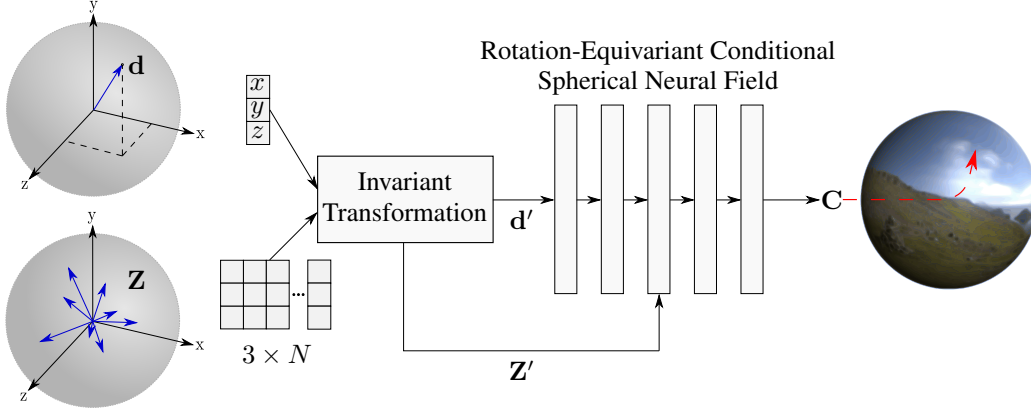


Figure 2: We propose to represent a space of spherical signals via a rotation-equivariant conditional spherical neural field. The signal in a direction \mathbf{d} can be queried by evaluation of the network and rotating the Vector Neuron conditioning latent code \mathbf{Z} , corresponds to rotating the spherical signal.

equivariance. Yu and Smith [59] seek to overcome this by rotation augmentation at training time, but this brute force approach makes no guarantee of rotation equivariance. Sztrajman et al. [49] separate environment maps into HDR and LDR components. Using a CNN-based auto-encoder for estimations of LDR components of lighting alongside a low dimensional SG model for the HDR lighting provided by the sun. They too require data augmentation in the form of rotations, can make no equivariance guarantees and, due to the low dimensionality of the SG model, struggle to represent environments with multiple HDR light sources.

Neural Fields Neural fields [57] have provided impressive results in a range of applications including representations of objects and scenes [44, 2, 33, 13, 12, 23, 36, 50], in inverse rendering [7, 5, 40, 48, 8, 61] and robotics [30, 11, 35]. The work most closely related to ours is Neural-PIL [8]. They use a FiLM SIREN similar to that proposed in Pi-GAN [10], and like us use a direction query vector and auto-decoder architecture. However, they do not have rotation-equivariance and apply no natural light prior. They also model pre-integrated lighting, conditioning the latter layers of their FiLM SIREN on a material roughness parameter.

Rotation Invariance/Equivariance Two important symmetries in computer vision are invariance and equivariance to the rotation group [9]. Some works attempt to achieve these properties via data augmentation [59, 37, 49], which still results in missed cases for continuous rotations. A solution alleviating the need for extensive data augmentation is the Vector Neuron [15], which offers a framework for designing $SO(3)$ -Equivariant networks via a latent matrix representation rather than a latent vector. This allows a direct mapping of rotations applied to the network’s input to its output, resulting in all possible rotations being explicitly represented via rotations of the latent codes.

Contribution We desire a representation of natural illumination environments that offers the following features. *Generative*: A generative model that captures the statistical regularities of natural illumination with a well-behaved latent space within which we can optimise to solve inverse problems. *Compact*: Reduces the dimensionality of inverse problems while preserving high-frequency lighting effects that are important for non-Lambertian appearance. *Rotation-Equivariant*: Respect the canonical orientation, i.e. any rotation of an environment about the vertical should be equally likely and equally well represented. *Statistical Prior*: Provides a prior to regularise inverse problems, or that can be sampled from for synthesis, only generating plausible illumination environments. *HDR*: Correctly handle HDR quantities essential for realistic rendering and the reproduction of natural light.

We introduce RENI - A Rotation-Equivariant Natural Illumination model. Our key contributions are:

- An extension of Vector Neurons to a rotation-equivariant neural field representation for spherical images, optionally restricted to rotations about the vertical axis.
- A variational autoencoder architecture for a generative model of spherical signals.

- The first natural, outdoor HDR illumination model.
- Evaluated in an inverse rendering task showing significant performance improvements over other lighting representations.

We choose to model scene radiance, i.e. environment lighting, directly as opposed to pre-integrated lighting with a particular BRDF. This makes our model more general since it can be used with arbitrary BRDFs at inference time or even for tasks other than rendering, such as to constrain shape from specular flow.

2 Rotation-Equivariant Conditional Spherical Neural Fields

We wish to construct a generative model of spherical signals that is rotation equivariant with respect to the latent representation of the signal. That is to say, a rotation of the latent representation corresponds to a rotation of a spherical signal and a signal can be reconstructed with exactly the same accuracy in any rotation. We begin by proposing a variant of Vector Neurons [15] for $SO(3)$ equivariant representation of spherical signals.

To achieve this, we use an ordered list of 3D vectors for our latent representation. Our model takes the form of a conditional spherical neural field, $f : S^2 \times \mathbb{R}^{3 \times N} \rightarrow \mathbb{R}^M$, such that $f(\mathbf{d}, \mathbf{Z})$ computes the value of the signal represented by latent code $\mathbf{Z} \in \mathbb{R}^{3 \times N}$ in direction $\mathbf{d} \in \mathbb{R}^3$, with $\|\mathbf{d}\| = 1$. For colour images, $M = 3$ and f outputs an RGB colour. By using a spherical neural field, we are agnostic to how the signals are sampled on the sphere. We can generate any sampling simply by choosing the grid of directions as appropriate. We also avoid boundary effects since our domain is continuous.

We construct the neural field such that it is *invariant* to a rotation of both \mathbf{d} and \mathbf{Z} simultaneously (i.e. $f(\mathbf{R}\mathbf{d}, \mathbf{R}\mathbf{Z}) = f(\mathbf{d}, \mathbf{Z})$ with $\mathbf{R} \in SO(3)$). This entails that the neural field is *equivariant* with respect to a rotation of \mathbf{Z} only (i.e. rotating \mathbf{Z} corresponds to rotating the spherical signal such that $f(\mathbf{d}, \mathbf{R}\mathbf{Z}) = f(\mathbf{R}^\top \mathbf{d}, \mathbf{Z})$).

Equivariant Transformation Key to our approach is a transformation of the inputs to the neural field, (\mathbf{d}, \mathbf{Z}) , such that they are rotation invariant. These divide into two parts: 1. \mathbf{d}' - the directional input to the spherical neural field and 2. \mathbf{Z}' - the latent code on which the neural field is conditioned.

The direction in which we wish to evaluate the spherical neural field must be encoded relative to the latent code in the particular rotation in which we encounter it. This is satisfied by using the inner product $\langle \mathbf{d}, \mathbf{Z} \rangle$, i.e. the matrix-vector product $\mathbf{d}' = \mathbf{Z}^\top \mathbf{d} \in \mathbb{R}^N$. Unlike Vector Neurons, our input is a direction not a position. Hence, the rotation invariant feature $\|\mathbf{d}\|$ conveys no information and we do not use it.

For the latent code, we follow the Vector Neurons invariant layer: $\mathbf{Z}' = \text{VN-In}(\mathbf{Z})$. However, we use the full Gram matrix $\mathbf{Z}^\top \mathbf{Z}$ since we expect the dimensionality of the latent space, N , to remain moderate for our data. If this $O(N^2)$ size becomes problematic, we can use the same scalable solution used by Vector Neurons [15].

Since our neural field is equivariant **we do not need to augment our training data over the space of rotations**. Observing a spherical signal once means we can reconstruct it with the same accuracy in any rotation.

Variational Auto-decoder We train our conditional spherical neural field as a decoder-only architecture, i.e. an auto-decoder [36]. This means that we optimise the network weights simultaneously with the latent codes for each training sample. This avoids the need to design a rotation-equivariant encoder while, for inverse tasks, only the decoder is needed so we avoid the redundancy of also training an encoder. However, training with no regularisation on the learnt latent space does not lead to a space that is smooth or that follows a known distribution. This means it cannot be sampled from, does not produce meaningful interpolations and provides no prior for inverse problems. For this reason, we use a *variational auto-decoder* [60] architecture. Each training sample is represented by a mean, $\boldsymbol{\mu}_i \in \mathbb{R}^{3N}$, and standard deviation, $\boldsymbol{\sigma}_i \in \mathbb{R}^{3N}$, that provide the parameters of a normal distribution from which the flattened latent code for that training sample is drawn: $\text{vec}(\mathbf{Z}_i) \sim \mathcal{N}(\boldsymbol{\mu}_i, \boldsymbol{\Sigma}_i)$, where $\boldsymbol{\Sigma}_i = \text{diag}(\sigma_{i,1}^2, \dots, \sigma_{i,3N}^2)$ is the diagonal covariance matrix. Using the reparameterisation

trick [28], we can generate a latent code $\text{vec}(\mathbf{Z}_i) = \boldsymbol{\mu}_i + \boldsymbol{\sigma}_i \odot \boldsymbol{\epsilon}$ where the noise is sampled as $\boldsymbol{\epsilon} \sim \mathcal{N}(\mathbf{0}, \mathbf{I}_{3N})$. During training, we optimise $\boldsymbol{\mu}_i$ and $\boldsymbol{\sigma}_i$ for each training sample and use the Kullback–Leibler divergence as a loss to regularise the distribution of each latent code toward the standard normal distribution:

$$\mathcal{L}_{\text{KLD}} = -\frac{1}{2} \sum_{i=1}^K \sum_{j=1}^{3N} (1 + \log(\sigma_{i,j}^2) - \mu_{i,j}^2 - \sigma_{i,j}^2), \quad (1)$$

where K is the number of training samples.

3 RENI: A Statistical Model of Natural Illumination

We now describe how to construct a statistical model of natural illumination environments as a restricted version of a rotation-equivariant conditional spherical neural field. We call our model RENI (Rotation-Equivariant Natural Illumination). In contrast to the full $SO(3)$ -equivariant formulation in Section 2, we propose a variant with only $SO(2)$ equivariance and explain in detail our training data, losses and implementation.

SO(2) Equivariance Natural environments have a canonical “up” direction (defined by gravity) but arbitrary rotation about this vertical axis. For this reason, we do not want arbitrary $SO(3)$ rotation equivariance. This would have the undesirable effect of permitting unnatural environment orientations (such as with the sky at the bottom), providing a less useful prior when solving inverse problems. So, we propose a restricted transformation of the neural field inputs that are invariant only to rotations, \mathbf{R}_y , about the vertical (y) axis.

In order to construct the invariant features, we use two selection matrices: \mathbf{S}_{xz} selects the components that are orthogonal to the axis of rotation (i.e. the x and z components) and are thus affected by a y -axis rotation, \mathbf{s}_y selects the unaffected y component:

$$\mathbf{S}_{xz} = \begin{bmatrix} 1 & 0 & 0 \\ 0 & 0 & 1 \end{bmatrix}, \quad \mathbf{s}_y = [0 \quad 1 \quad 0]$$

The directional part of the invariant input now contains three components: $\mathbf{d}' = (\mathbf{s}_y \mathbf{d}, \langle \mathbf{S}_{xz} \mathbf{d}, \mathbf{S}_{xz} \mathbf{Z} \rangle, \|\mathbf{S}_{xz} \mathbf{d}\|)$. The first is the invariant component of \mathbf{d} . The second encodes \mathbf{d} relative to \mathbf{Z} in the x - z plane. The third measures the norm of \mathbf{d} projected into the x - z plane which is unchanged by rotations about y .

The conditioning part of the invariant input now contains two components: $\text{VN-In}(\mathbf{Z}) = \mathbf{Z}' = (\mathbf{s}_y \mathbf{Z}, (\mathbf{S}_{xz} \mathbf{Z})^\top \mathbf{S}_{xz} \mathbf{Z})$. The first is simply the invariant component of each column of \mathbf{Z} . The second is the invariant transformation (Gram matrix) of latent vectors projected into the x - z plane.

Reconstruction Loss and HDR HDR imaging is essential for realistic rendering and enables the accurate representation of the full dynamic range of natural light. Therefore our model must learn an HDR representation of natural illumination. Computing a reconstruction loss in linear HDR space is dominated by large values and leads to poor reconstruction of most of the environment. Therefore, similar to [18], we train our network to output $\log(\text{HDR})$ values and compute the reconstruction loss in log space. We further normalise the $\log(\text{HDR})$ values to the range $[-1, 1]$ by scaling and shifting using the maximum and minimum values across the whole training set.

Each training sample comprises P pairs of directions and corresponding normalised $\log(\text{HDR})$ RGB colours that we store in the matrices $\mathbf{D}_i = [\mathbf{d}_{i1}, \dots, \mathbf{d}_{iP}] \in \mathbb{R}^{3 \times P}$ and $\mathbf{C}_i = [\mathbf{c}_{i1}, \dots, \mathbf{c}_{iP}] \in \mathbb{R}^{3 \times P}$ respectively. RENI is agnostic to the resolution and sampling of the spherical signal. The neural field can be queried for any direction. In practice, our dataset contains spherical images in an equirectangular sampling containing $P = 2H^2$ pixels where H is the height of the images. Since equirectangular images are irregularly sampled, we weight the mean squared reconstruction loss by the sine of the polar angle, $\theta(\mathbf{d})$:

$$\mathcal{L}_{\text{recon}} = \sum_{i=1}^K \frac{1}{P} \sum_{j=1}^P \sin(\theta(\mathbf{d}_{ij})) \|f(\mathbf{d}_{ij}) - \mathbf{c}_{ij}\|^2 \quad (2)$$

Neural Field Our neural field, f , is implemented as a SIREN [44] - an MLP with a periodic activation function. This architecture has proven highly effective at representing a wide range of complex natural signals. In order to condition the SIREN on the invariant latent code \mathbf{Z}' , we use *conditioning-by-concatenation* [44, 57], i.e. we simply input both \mathbf{d}' and \mathbf{Z}' to the network. We also tested a FiLM-conditioned SIREN [10] but could not get significant performance improvements and, perhaps due to the small size of our dataset, FiLM conditioning resulted in a non-smooth latent space that could drastically affect performance when fitting to unseen images.

Training Data We have curated a dataset of 1,694 HDR equirectangular images of outdoor, natural illumination environment obtained with either CC0 1.0 Universal Public Domain Dedication license [24, 19, 27] or with written permission to redistribute a low-resolution version of their dataset [25, 1, 45, 51]. All images were then checked to ensure they did not contain any personally identifiable information or offensive content and any images that contained predominantly unnatural light sources were removed. 21 images were also selected and held back for optimising only the latent codes at test time, resulting in a training dataset of 1,673 HDR images.

Training We use Adam [29] to optimise the sum of the reconstruction and KLD losses:

$$\mathcal{L}_{\text{Train}} = \mathcal{L}_{\text{recon}} + \frac{\beta}{D} \mathcal{L}_{\text{KLD}} \quad (3)$$

where β is a hyperparameter to weight the KLD loss and $D = 3N$ is the dimensionality of the latent space, used to normalise for the choice of N . We randomly initialise the mean latent code for each image, μ_i , from a standard normal distribution. In order to ensure the positivity of the variances, $\sigma_{i,j}^2$, we optimise $\log(\sigma_{i,j}^2)$ which we initialise randomly from a normal distribution with mean -5 and variance 1. We use all the pixels from a single training image as a mini-batch and use batch size 1.

In order to speed up training, we employ a progressive strategy. We start by training with low resolution ($H = 16$) images and double resolution every 800 epochs until we reach $H = 128$ resolution for a total of 2,400 epochs. This allows the network to quickly learn low-frequency features, gradually obtaining higher frequency details later in the training. Unlike with a convolutional architecture, the spatially-continuous nature of the neural field means we can implement multi-resolution training using a single network. We simply upsample the grid of directions, \mathbf{D}_i , and increase the resolution of the target equirectangular images to match this resolution.

We used Weights and Biases [6] for experiment tracking, visualisations and hyper-parameter grid search. This yielded the best performance using a variational auto-decoder, SIREN with 5 layers each with 128 hidden features. We use an exponentially decaying learning rate starting at 10^{-5} and decreasing to 10^{-7} by the end of training and weight the KLD loss $\beta = 10^{-4}$ to be of similar magnitude to the reconstruction loss. Training RENI with a latent code dimension of $D = 27$, took around 15 hours on a local Nvidia A40 48GB GPU.

Model Fitting At test time, the SIREN network is held static, and only latent codes are optimised in order to fit to an unseen image. We initialise the latent code to zeros, corresponding to the mean environment map (see Figure 1, left). This provides an unbiased initialisation in the absence of any prior information about the environment. We found performance on test images was improved by including a cosine similarity loss $\mathcal{L}_{\text{Cosine}}$ on the RGB colour vectors [32] weighted using the same $\sin(\theta(\mathbf{d}))$ weight as used in $\mathcal{L}_{\text{recon}}$. We also include a prior loss on the latent vector $\mathcal{L}_{\text{Prior}} = \|\mathbf{Z}\|_{\text{Fro}}^2$. Our test time loss is therefore:

$$\mathcal{L}_{\text{Test}} = \mathcal{L}_{\text{recon}} + \rho \mathcal{L}_{\text{Cosine}} + \gamma \mathcal{L}_{\text{Prior}}. \quad (4)$$

We again use a multi-resolution training scheme, fitting with the same resolutions and number of epochs as used during training. A hyper-parameter grid search found the best performance when using $\rho = 10^{-4}$, $\gamma = 10^{-7}$, and an exponentially decaying learning rate starting at 10^{-2} and decreasing to 10^{-4} .

A PyTorch implementation, our dataset and trained models can be found at [jadgardner.github.io/RENI](https://github.com/jadgardner.github.io/RENI).

4 Evaluation

Generalisation We begin by evaluating the generalisation performance of RENI when approximating unseen environments. We compare against SH and SG and explore how generalisation performance varies as a function of latent code dimension. We consider RGB spherical harmonics of order 2, 5, 6 and 9 equal to latent code dimension $D = 3 \times N$ for $N = 9, 36, 49, 100$. Since SG requires a dimensionality that is a multiple of 6, where D is not a multiple of 6, we bias in SGs favour by using the next multiple, i.e. $\lceil D/6 \rceil \cdot 6$. We used an open-source implementation of per-pixel environment map fitting provided by [31] to fit our SG models. As shown in Figure 3, RENI can capture higher frequency detail than both SH and SG, is less dominated by high-value pixels and can reproduce accurate HDR values. A comparison of the mean PSNR across the test set images for increasing latent code dimensionality is shown in Table 1.

Table 1: The mean PSNR when fitting to the test set for increasing latent dimensions. Where an exact dimensionality comparison is not possible for SG the dimensionality used is shown in brackets.

D	RENI	SH	SG
27	17.02	12.80	16.04 ($N = 30$)
108	19.58	15.89	18.44
147	19.97	16.44	19.26 ($N = 150$)
300	20.47	17.07	20.02

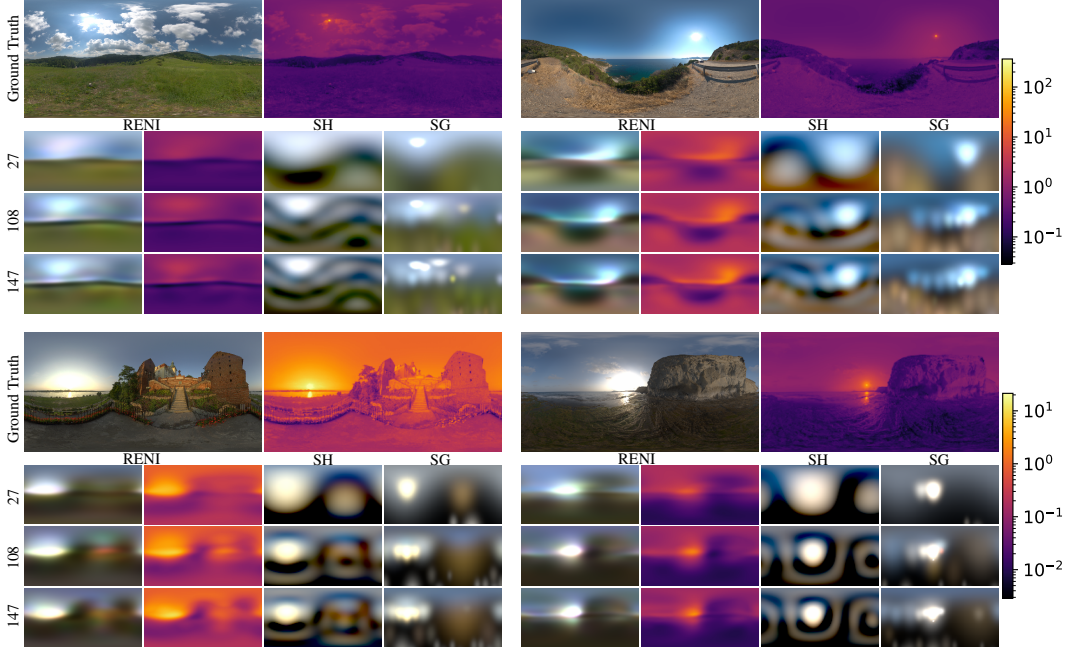


Figure 3: Generalisation to unseen images with latent code dimensions, $D = 3N$ for $N = 9, 36, 49$ and for SH of equal dimensionality (orders 2, 5, and 6). SG results are with dimensionality $D = 30, 108, 150$. Heat maps with log-scale colour bars for ground truth and RENI are also shown.

To test the impact of restricting RENI’s equivariance to $SO(2)$ we ran an ablation of models with $SO(3)$, $SO(2)$ and without equivariance at three sizes of latent code dimension D . For the model without equivariance, we augmented the dataset with rotations of the images at increments of 0.785rad for a training dataset size of 13384 images. The $SO(2)$ case performs best for all latent code sizes, and both the $SO(2)$ and $SO(3)$ outperform the model trained purely using augmentation whilst using significantly less data. Results are shown in Table 2.

Table 3 shows an ablation of model sizes. When using a smaller network, reconstruction quality suffers due to the representational power of the network being reduced. Whereas the larger networks over-fit on the training data and optimising latent codes to fit unseen images becomes more challenging, perhaps due to the small size of the dataset.

Table 2: Mean PSNR on the test set for models with varying levels of equivariance.

D	None	SO(2)	SO(3)
27	11.32	17.02	14.00
108	15.85	19.58	18.27
147	14.64	19.97	17.45

Table 3: Mean PSNR on the test set for different network sizes and latent dimensionality.

Layers	$D = 27$	$D = 108$	$D = 147$
3	16.25	18.29	18.57
5	17.02	19.58	19.97
7	16.38	18.13	18.15

Latent Space Interpolation As shown in Figure 4, linear interpolations between codes result in smooth transitions between images and plausible natural environments for all intermediate latent codes showing how RENI encodes a meaningful internal representation of natural illumination.



Figure 4: Interpolation results for RENI with latent code dimension of $D = 108$. Rows 1 and 2 show interpolations between two random latent codes, and row 3 shows an interpolation between two training images with the ground-truth images shown.

Environment Completion Any picture of a natural scene contains cues about the surrounding environment that the scene was captured in, such as likely sun locations and possible environmental content. If RENI is only provided with a small portion of the complete environment map in its loss at test time, RENI can hallucinate plausible completions of the environment. As shown in Figure 5, RENI makes sensible estimations about the possible colours and shapes of land and sky and often predicts quite accurate sun locations despite the sun being outside the image crop.

Inverse Rendering To test the performance of RENI in an inverse rendering pipeline, we implemented a normalised Blinn-Phong environment map shader in PyTorch3D, enabling fully differentiable rendering. We render a 3D object with fixed geometry, pose, camera and material parameters such that only lighting in the scene is unknown. Optimising only latent codes, we minimise the same losses as used in \mathcal{L}_{Test} , without the $\sin(\theta(d))$ weighting needed for equirectangular images, between a rendering using a ground truth environment map and a one using the output of RENI. This was tested for incremental increases in weighting of the Blinn-Phong specular term (K_s), from $K_s = 0$ to $K_s = 1.0$ in steps of 0.2. A normalisation factor $\alpha = (n + 2)/(4\pi(2 - e(\frac{-n}{2})))$ [21], was applied to K_s to get a steady transition from diffuse to specular. We achieved the best performance using $\alpha = 10^3$, $\gamma = 10^{-4}$, and an exponentially decaying learning rate starting at 10^{-2} and decreasing to 10^{-4} over 2,400 epochs. We use an environment map resolution of $H = 64$ and render the object with a resolution of 128^2 . In Figure 6 we compare against SH environment maps computed in closed form using linear least squares for increasing specularity. As expected, SH performs well at producing accurate renders of diffuse objects. However, the environment maps produced are unnatural, and as the specular term increases in weight, SH degrades in performance significantly compared to RENI.

Non-convexity of Reconstruction Error in Latent Space RENI is rotation equivariant. However, this does not necessarily mean that optimising to fit a rotated image will yield a rotated version of the latent code resulting from fitting to an unrotated version of the image. This means that the loss landscape of our reconstruction losses is not convex. To verify this, we fit RENI to a version of the test set containing pairs of unseen images rotated 180 degrees apart. Initialising at the mean environment and optimising resulted in pairs of latent codes $\mathbf{Z}_1, \mathbf{Z}_2$. Ideally, this would result in each latent code being explained via a y -axis rotation of the other. To test this we minimised \mathbf{M} for $\|\mathbf{Z}_1\mathbf{M} - \mathbf{Z}_2\|_2$ and obtained a rotation matrix \mathbf{R} that minimises $\|\mathbf{M} - \mathbf{R}\|_F$. We then calculate the

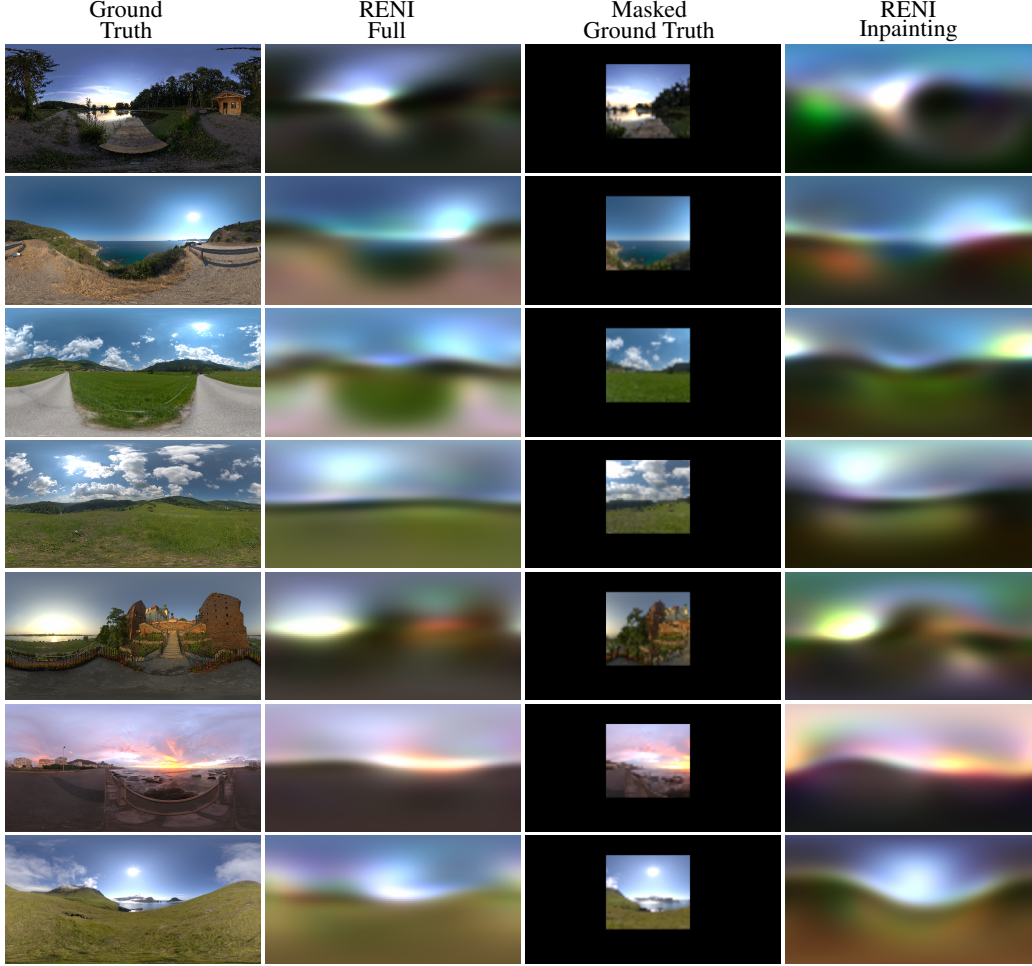


Figure 5: Col. 2 shows the output of optimising latent codes on full ground-truth (Col. 1). When trained on a masked ground-truth (Col. 3) RENI predicts plausible continuations for the environment and makes accurate estimations of sun locations (Col. 4). Results from a $D = 108$ model.

relative error between \mathbf{RZ}_1 and \mathbf{Z}_2 :

$$E = \frac{\|\mathbf{RZ}_1 - \mathbf{Z}_2\|_F}{\|\mathbf{Z}_2\|_F}$$

For a model of $D = 27$, this resulted in $E < 2.0\%$ for 18 of the 21 image pairs, demonstrating that both latent codes can largely be explained as a simple rotation of the other. However, for the remaining three images, the error was higher, suggesting there is redundancy in the latent space, i.e. there are multiple possible explanations for a single image. Better latent space regularisation, tuning model dimensionality and a larger dataset might help resolve this.

5 Discussion and Conclusion

We introduced rotation-equivariant spherical neural fields and used them to create RENI, a natural illumination prior. Demonstrating how random samples from RENI always produce plausible illumination maps and RENI’s usefulness for environment completion and inverse rendering. There are many exciting avenues for future research, for example, implementing RENI in larger inverse rendering pipelines where it could be a simple drop-in replacement for SH and using RENI for LDR to HDR image reconstruction. Furthermore, our spherical neural field is the initial step towards a Generative Adversarial Network [20] (GAN) for spherical signals and could be used as the generator alongside a Spherical CNN [14] for the discriminator in a GAN framework.

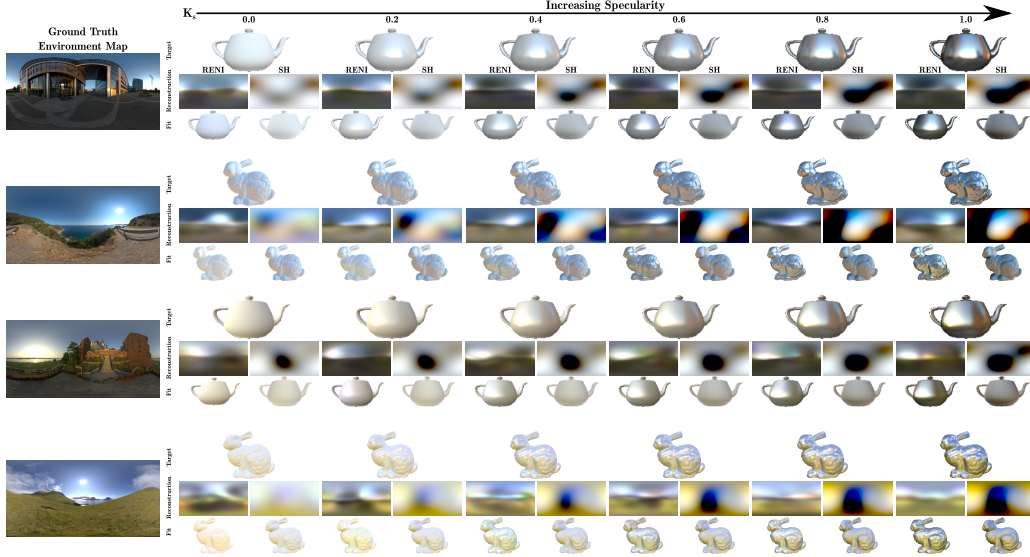


Figure 6: Reconstruction results in an inverse rendering task. The specular Blinn-Phong term K_s increases from left to right in steps of 0.2. Both RENI and SH have a dimensionality of $D = 27$. SH performs well in the purely diffuse case, but the resulting environment map reconstruction is unnatural, and as K_s increases RENI performs significantly better.

Limitations Using the Gram matrix for the invariant representation, which is $O(n^2)$, limits the size of the latent code you can realistically use. This could be addressed through the use of the invariant layer proposed by [15] to reduce this to $O(n)$. The very highest frequency detail is still not resolved even when using larger latent code sizes; scaling up with a larger dataset and network size is likely to address this. Because RENI has a prior for natural illumination, unlike SH, RENI’s performance decreases when fit to indoor scenes. Interestingly, RENI still generalises to indoor scenes quite well; see supplementary material for examples of RENI fitting to indoor scenes.

Human vision has complex interactions between illumination, geometry and texture priors. For example, the Hollow Face Illusion [26] arises from face geometry priors overriding the lighting from above illumination prior; while in the Bas relief ambiguity [4], geometric priors cause incorrect lighting estimation. Our model discounts these interactions, learning an illumination prior independently but not its interactions with other cues.

We strictly allow only $SO(2)$ equivariance. However, considering typical camera coordinate systems, the up axis will sometimes not align with gravity when the camera is pointed up or down. For inverse problems, this would mean the gravity vector would need to be explicitly estimated (an accelerometer would resolve this). Alternatively, we could build our model with full $SO(3)$ equivariance but then learn a prior over the space of camera poses relative to gravity.

Broader Impact The illumination prior presented here has the potential to improve the performance of inverse rendering pipelines, of which there are both positive and negative downstream use cases that should be considered; for example, the generation of highly realistic 3D models of a person’s likeness without their consent. Advances in inverse and neural rendering could potentially lead to employment loss in the generation of 3D assets. However, we are optimistic that the democratisation of 3D model generation will be a value-generating technology for the large majority. The illumination prior might be biased since most of the available and used HDR images were captured in Europe.

Acknowledgments and Disclosure of Funding James Gardner was supported by the EPSRC Centre for Doctoral Training in Intelligent Games & Games Intelligence (IGGI) (EP/S022325/1). We would like to thank the attendees of Dagstuhl Seminar, 22121 - 3D Morphable Models and Beyond, for their valuable insights and discussions around this work.

References

- [1] Whitemagus 3D. *HDRIs • Whitemagus 3D Models*. en-US. URL: <http://www.whitemagus3dmodels.com>.
- [2] Matan Atzmon and Yaron Lipman. “SAL: Sign Agnostic Learning of Shapes from Raw Data”. In: *IEEE/CVF Conference on Computer Vision and Pattern Recognition (CVPR)*. 2020.
- [3] R. Basri and D.W. Jacobs. “Lambertian reflectance and linear subspaces”. In: *IEEE Transactions on Pattern Analysis and Machine Intelligence* 25.2 (2003), pp. 218–233.
- [4] Peter N. Belhumeur, David J. Kriegman, and Alan L. Yuille. “The Bas-Relief Ambiguity”. In: *International Journal of Computer Vision* 35.1 (Nov. 1999), pp. 33–44.
- [5] Sai Bi, Zexiang Xu, Pratul Srinivasan, Ben Mildenhall, Kalyan Sunkavalli, Miloš Hašan, Yannick Hold-Geoffroy, David Kriegman, and Ravi Ramamoorthi. “Neural Reflectance Fields for Appearance Acquisition”. In: *arXiv*. 2020.
- [6] Lukas Biewald. *Experiment Tracking with Weights and Biases*. 2020. URL: <https://www.wandb.com/>.
- [7] Mark Boss, Raphael Braun, Varun Jampani, Jonathan T. Barron, Ce Liu, and Hendrik P. A. Lensch. “NeRD: Neural Reflectance Decomposition from Image Collections”. In: *IEEE International Conference on Computer Vision (ICCV)*. 2021.
- [8] Mark Boss, Varun Jampani, Raphael Braun, Ce Liu, Jonathan T. Barron, and Hendrik P. A. Lensch. “Neural-PIL: Neural Pre-Integrated Lighting for Reflectance Decomposition”. In: *Advances in Neural Information Processing Systems (NeurIPS)*. 2021.
- [9] Michael M. Bronstein, Joan Bruna, Taco Cohen, and Petar Veličković. *Geometric Deep Learning: Grids, Groups, Graphs, Geodesics, and Gauges*. 2021.
- [10] Eric R. Chan, Marco Monteiro, Petr Kellnhofer, Jiajun Wu, and Gordon Wetzstein. “pi-GAN: Periodic Implicit Generative Adversarial Networks for 3D-Aware Image Synthesis”. In: *2021 IEEE/CVF Conference on Computer Vision and Pattern Recognition (CVPR)*. 2021.
- [11] Boyuan Chen, Robert Kwiatkowski, Carl Vondrick, and Hod Lipson. “Full-Body Visual Self-Modeling of Robot Morphologies”. In: *Science Robotics* 7.68 (2021).
- [12] Zhiqin Chen and Hao Zhang. “Learning Implicit Fields for Generative Shape Modeling”. In: *2019 IEEE/CVF Conference on Computer Vision and Pattern Recognition (CVPR)*. 2019.
- [13] Julian Chibane, Aymen Mir, and Gerard Pons-Moll. “Neural Unsigned Distance Fields for Implicit Function Learning”. In: *Advances in Neural Information Processing Systems (NeurIPS)*. 2020.
- [14] Taco S. Cohen, Mario Geiger, Jonas Köhler, and Max Welling. “Spherical CNNs”. In: *International Conference on Learning Representations*. 2018.
- [15] Congyue Deng, Or Litany, Yueqi Duan, Adrien Poulénard, Andrea Tagliasacchi, and Leonidas Guibas. “Vector Neurons: A General Framework for SO(3)-Equivariant Networks”. In: *IEEE International Conference on Computer Vision (ICCV)*. Apr. 2021.
- [16] Ron O. Dror, Alan S. Willsky, and Edward H. Adelson. “Statistical characterization of real-world illumination”. In: *Journal of Vision* 4.9 (Sept. 2004), pp. 11–11.
- [17] Bernhard Egger, Sandro Schönborn, Andreas Schneider, Adam Kortylewski, Andreas Morel-Forster, Clemens Blumer, and Thomas Vetter. “Occlusion-Aware 3D Morphable Models and an Illumination Prior for Face Image Analysis”. In: *International Journal of Computer Vision* 126 (2018), pp. 1269–1287.
- [18] Gabriel Eilertsen, Joel Kronander, Gyorgy Denes, Rafal K. Mantiuk, and Jonas Unger. “HDR Image Reconstruction from a Single Exposure Using Deep CNNs”. In: *ACM Trans. Graph.* 36.6 (Nov. 2017). Place: New York, NY, USA Publisher: Association for Computing Machinery.
- [19] GiantCowFilms. *HDRIs • GiantCowFilms*. en-US. URL: <https://giantcowfilms.com/category/hdri/>.
- [20] Ian Goodfellow, Jean Pouget-Abadie, Mehdi Mirza, Bing Xu, David Warde-Farley, Sherjil Ozair, Aaron Courville, and Yoshua Bengio. “Generative Adversarial Nets”. In: *Advances in Neural Information Processing Systems*. Ed. by Z. Ghahramani, M. Welling, C. Cortes, N. Lawrence, and K. Q. Weinberger. Vol. 27. Curran Associates, Inc., 2014.
- [21] Yoshiharu Gotanda, Naty Hoffman, Adam Martinez, and Ben Snow. “Physically-Based Shading in Film and Game Production”. In: *ACM SIGGRAPH 2010 Courses*. SIGGRAPH ’12. Association for Computing Machinery, 2010.

- [22] Robin Green. “Spherical harmonic lighting: The gritty details”. In: *Archives of the game developers conference*. Vol. 56. 2003, p. 4.
- [23] Amos Gropp, Lior Yariv, Niv Haim, Matan Atzmon, and Yaron Lipman. “Implicit Geometric Regularization for Learning Shapes”. In: *Proceedings of Machine Learning and Systems*. 2020.
- [24] Poly Haven. *HDRIs • Poly Haven*. URL: <https://polyhaven.com/hdri/>.
- [25] hdrmaps. *HDRIs • hdrmaps*. en-US. URL: <https://hdrmaps.com/>.
- [26] Harold Hill and Vicki Bruce. “Independent Effects of Lighting, Orientation, and Stereopsis on the Hollow-Face Illusion”. In: *Perception* 22.8 (1993), pp. 887–897.
- [27] iHDRI. *HDRIs • iHDRI*. URL: <https://www.ihdri.com/hdri-skies-outdoor/>.
- [28] Diederik P Kingma and Max Welling. “Auto-Encoding Variational Bayes”. In: *International Conference on Learning Representations (ICLR)*. 2013. DOI: 10.48550/ARXIV.1312.6114.
- [29] Diederik P. Kingma and Jimmy Ba. “Adam: A Method for Stochastic Optimization”. In: *International Conference on Learning Representations (ICLR)* (2015).
- [30] Yunzhu Li, Shuang Li, Vincent Sitzmann, Pulkit Agrawal, and Antonio Torralba. “3D Neural Scene Representations for Visuomotor Control”. In: *Conference on Robot Learning (CoRL)*. 2021.
- [31] Zhengqin Li, Mohammad Shafiei, Ravi Ramamoorthi, Kalyan Sunkavalli, and Manmohan Chandraker. “Inverse rendering for complex indoor scenes: Shape, spatially-varying lighting and svbrdf from a single image”. In: *Proceedings of the IEEE/CVF Conference on Computer Vision and Pattern Recognition*. 2020, pp. 2475–2484.
- [32] Demetris Marnerides, Thomas Bashford-Rogers, Jonathan Hatchett, and Kurt Debattista. “ExpandNet: A Deep Convolutional Neural Network for High Dynamic Range Expansion from Low Dynamic Range Content”. In: *Computer Graphics Forum* 37 (2018).
- [33] Lars Mescheder, Michael Oechsle, Michael Niemeyer, Sebastian Nowozin, and Andreas Geiger. “Occupancy Networks: Learning 3D Reconstruction in Function Space”. In: *Proceedings IEEE Conf. on Computer Vision and Pattern Recognition (CVPR)*. 2019.
- [34] Ren Ng, Ravi Ramamoorthi, and Pat Hanrahan. “All-Frequency Shadows Using Non-Linear Wavelet Lighting Approximation”. In: *ACM SIGGRAPH 2003 Papers*. SIGGRAPH ’03. Association for Computing Machinery, 2003, pp. 376–381.
- [35] Joseph Ortiz, Alexander Clegg, Jing Dong, Edgar Sucar, David Novotny, Michael Zollhoefer, and Mustafa Mukadam. “iSDF: Real-Time Neural Signed Distance Fields for Robot Perception”. en. In: *Robotics: Science and Systems* (May 2022).
- [36] Jeong Joon Park, Peter Florence, Julian Straub, Richard Newcombe, and Steven Lovegrove. “DeepSDF: Learning Continuous Signed Distance Functions for Shape Representation”. In: *Computer Vision & Pattern Recognition (CVPR)*. 2019.
- [37] Charles R Qi, Hao Su, Kaichun Mo, and Leonidas J Guibas. “Pointnet: Deep learning on point sets for 3d classification and segmentation”. In: *Proceedings of the IEEE conference on computer vision and pattern recognition*. 2017, pp. 652–660.
- [38] Ravi Ramamoorthi and Pat Hanrahan. “An efficient representation for irradiance environment maps”. In: *Proceedings of the 28th annual conference on Computer graphics and interactive techniques*. SIGGRAPH ’01. Association for Computing Machinery, Aug. 2001, pp. 497–500.
- [39] Ravi Ramamoorthi and Pat Hanrahan. “Frequency Space Environment Map Rendering”. In: *Proceedings of the 29th Annual Conference on Computer Graphics and Interactive Techniques*. SIGGRAPH ’02. Association for Computing Machinery, 2002, pp. 517–526.
- [40] Viktor Rudnev, Mohamed Elgharib, William Smith, Lingjie Liu, Vladislav Golyanik, and Christian Theobalt. “NeRF for Outdoor Scene Relighting”. In: *European Conference on Computer Vision (ECCV)*. 2022.
- [41] Soumyadip Sengupta, Jinwei Gu, Kihwan Kim, Guilin Liu, David W. Jacobs, and Jan Kautz. “Neural Inverse Rendering of an Indoor Scene from a Single Image”. In: *International Conference on Computer Vision (ICCV)*. 2019.
- [42] Soumyadip Sengupta, Angjoo Kanazawa, Carlos D. Castillo, and David Jacobs. “SfSNet: Learning Shape, Reflectance and Illuminance of Faces in the Wild”. In: *Computer Vision and Pattern Recognition (CVPR)*. 2018.
- [43] Zhixin Shu, Ersin Yumer, Sunil Hadap, Kalyan Sunkavalli, Eli Shechtman, and Dimitris Samaras. *Neural Face Editing with Intrinsic Image Disentangling*. 2017.

- [44] Vincent Sitzmann, Julien Martel, Alexander Bergman, David Lindell, and Gordon Wetzstein. “Implicit neural representations with periodic activation functions”. In: *Adv. Neural Inf. Process. Syst.* 33 (2020), pp. 7462–7473.
- [45] HDRI Skies. *HDRI • HDRI Skies*. en-US. URL: <https://hdri-skies.com/>.
- [46] Peter-Pike Sloan, Jan Kautz, and John Snyder. “Precomputed Radiance Transfer for Real-Time Rendering in Dynamic, Low-Frequency Lighting Environments”. en. In: *ACM Transactions on Graphics* 21.3 (2002), p. 10.
- [47] Shuran Song and Thomas Funkhouser. “Neural Illumination: Lighting Prediction for Indoor Environments”. In: *IEEE Conference on Computer Vision and Pattern Recognition*. 2019.
- [48] Pratul P. Srinivasan, Boyang Deng, Xiuming Zhang, Matthew Tancik, Ben Mildenhall, and Jonathan T. Barron. “NeRV: Neural Reflectance and Visibility Fields for Relighting and View Synthesis”. In: *IEEE/CVF Conference on Computer Vision and Pattern Recognition (CVPR)*. 2020.
- [49] Alejandro Sztrajman, Alexandros Neophytou, Tim Weyrich, and Eric Sommerlade. “High-Dynamic-Range Lighting Estimation From Face Portraits”. In: *2020 International Conference on 3D Vision (3DV)*. 2020, pp. 355–363.
- [50] Matthew Tancik, Vincent Casser, Xincheng Yan, Sabeek Pradhan, Ben Mildenhall, Pratul P. Srinivasan, Jonathan T. Barron, and Henrik Kretschmar. “Block-NeRF: Scalable Large Scene Neural View Synthesis”. In: *arXiv*. 2022.
- [51] textures. *HDRI • textures*. URL: <https://www.textures.com/>.
- [52] Rhiannon Thomas, Marko Nardini, and Denis Mareschal. “Interactions between “light-from-above” and convexity priors in visual development”. In: *Journal of Vision* 10.8 (July 2010), pp. 6–6.
- [53] Yu-Ting Tsai and Zen-Chung Shih. “All-Frequency Precomputed Radiance Transfer using Spherical Radial Basis Functions and Clustered Tensor Approximation”. In: *Association for Computing Machinery* 25.3 (2006), p. 10.
- [54] Jiaping Wang, Peiran Ren, Minmin Gong, John Snyder, and Baining Guo. “All-Frequency Rendering of Dynamic, Spatially-Varying Reflectance”. In: *Association for Computing Machinery* 28.5 (2009), p. 10.
- [55] Yang Wang, Lei Zhang, Zicheng Liu, Gang Hua, Zhen Wen, Zhengyou Zhang, and Dimitris Samaras. “Face Relighting from a Single Image under Arbitrary Unknown Lighting Conditions”. In: *IEEE transactions on pattern analysis and machine intelligence* 31 (Nov. 2009), pp. 1968–84.
- [56] Zian Wang, Jonah Philion, Sanja Fidler, and Jan Kautz. “Learning Indoor Inverse Rendering with 3D Spatially-Varying Lighting”. In: *Proceedings of International Conference on Computer Vision (ICCV)*. 2021.
- [57] Yiheng Xie, Towaki Takikawa, Shunsuke Saito, Or Litany, Shiqin Yan, Numair Khan, Federico Tombari, James Tompkin, Vincent Sitzmann, and Srinath Sridhar. “Neural Fields in Visual Computing and Beyond”. In: *Computer Graphics Forum (Eurographics 2022)* (Nov. 2021).
- [58] Ye Yu, Abhimettra Meka, Mohamed Elgharib, Hans-Peter Seidel, Christian Theobalt, and Will Smith. “Self-supervised Outdoor Scene Relighting”. In: *European Conference on Computer Vision (ECCV)*. 2020.
- [59] Ye Yu and William A. P. Smith. “Outdoor inverse rendering from a single image using multi-view self-supervision”. In: *IEEE Transactions on Pattern Analysis and Machine Intelligence*. 2021.
- [60] Amir Zadeh, Yao-Chong Lim, Paul Pu Liang, and Louis-Philippe Morency. “Variational Auto-Decoder: A Method for Neural Generative Modeling from Incomplete Data”. In: *arXiv*. 2021.
- [61] Kai Zhang, Fujun Luan, Qianqian Wang, Kavita Bala, and Noah Snavely. “PhySG: Inverse Rendering with Spherical Gaussians for Physics-based Material Editing and Relighting”. In: *The IEEE/CVF Conference on Computer Vision and Pattern Recognition (CVPR)*. 2021.

Rotation-Equivariant Conditional Spherical Neural Fields for Learning a Natural Illumination Prior

-Supplementary Material-

James A. D. Gardner
Department of Computer Science
University of York
York, United Kingdom
james.gardner@york.ac.uk

Bernhard Egger
Cognitive Computer Vision Lab
Friedrich-Alexander-Universität
Erlangen, Germany
bernhard.egger@fau.de

William A. P. Smith
Department of Computer Science
University of York
York, United Kingdom
william.smith@york.ac.uk

Here we provide further results, additional training information, and explore the how RENI performs when fit to illumination maps that contain unnatural illumination conditions.

A Additional Training Details

A.1 Cosine Loss

When optimising just the latent codes to unseen environment maps, we found improved performance when including a cosine similarity loss. As with $\mathcal{L}_{\text{recon}}$ this was weighted by the sine of the polar angle, $\theta(\mathbf{d})$, to compensate for the irregular sampling of equirectangular images. Each training sample comprises P pairs of directions and corresponding normalised log(HDR) RGB colours that we store in the matrices $\mathbf{D}_i = [\mathbf{d}_{i1}, \dots, \mathbf{d}_{iP}] \in \mathbb{R}^{3 \times P}$ and $\mathbf{C}_i = [\mathbf{c}_{i1}, \dots, \mathbf{c}_{iP}] \in \mathbb{R}^{3 \times P}$ respectively. $\mathcal{L}_{\text{Cosine}}$ is therefore defined as:

$$\mathcal{L}_{\text{Cosine}} = \sum_{i=1}^K \left(1 - \frac{1}{P} \sum_{j=1}^P \sin(\theta(\mathbf{d}_{ij})) \frac{f(\mathbf{d}_{ij}) \cdot \mathbf{c}_{ij}}{\max(\|f(\mathbf{d}_{ij})\|_2 \cdot \|\mathbf{c}_{ij}\|_2, \varepsilon)} \right) \quad (1)$$

where K is the number of training samples.

We used a value of $\varepsilon = 10^{-20}$ to prevent singularities. This loss is used again during the inverse rendering task. However as the images used in that loss are not equirectangular the $\sin(\theta(\mathbf{d}))$ term is not included.

A.2 Gamma Correction

For display, all linear HDR images \mathbf{I} had their gamma adjusted using the following process:

1. Adjust exposure to set the white level to the p -th percentile ($p = 98$)

$$\mathbf{I} \leftarrow \frac{\mathbf{I}}{\text{percentile}(\mathbf{I}, p)}$$

2. Clamp between $[0, 1]$

$$\mathbf{I} \leftarrow \text{clamp}(\mathbf{I}, 0, 1)$$

3. Apply gamma correction using the standard sRGB gamma curve:

$$\gamma_{RGB}(\mathbf{I}) = \begin{cases} 12.92\mathbf{I} & \mathbf{I} \leq 0.0031308 \\ 1.055\mathbf{I}^{1/2.4} - 0.055 & \mathbf{I} > 0.0031308 \end{cases}$$

such that:

$$\mathbf{I} \leftarrow \gamma_{RGB}(\mathbf{I})$$

B Additional Results

We include additional qualitative results of the RENI model. Figures 1 and 2 show further examples from the selection of test images demonstrating how RENI performs against SH and SG for increasing latent dimensionality. Figure 3 demonstrates performance differences between RENI and SH at the environment completion task. RENI’s prior on natural illumination enables significantly more realistic results and no over-fitting to the provided cutout. Figures 4 and 5 show a $D = 108$ model fitting to unseen images that contain unnatural illuminations, e.g. artificial illuminations or indoor environments. Figure 6 shows a comparison between RENI and SG in the inverse rendering task and Figure 7 shows one of RENI’s failure cases.

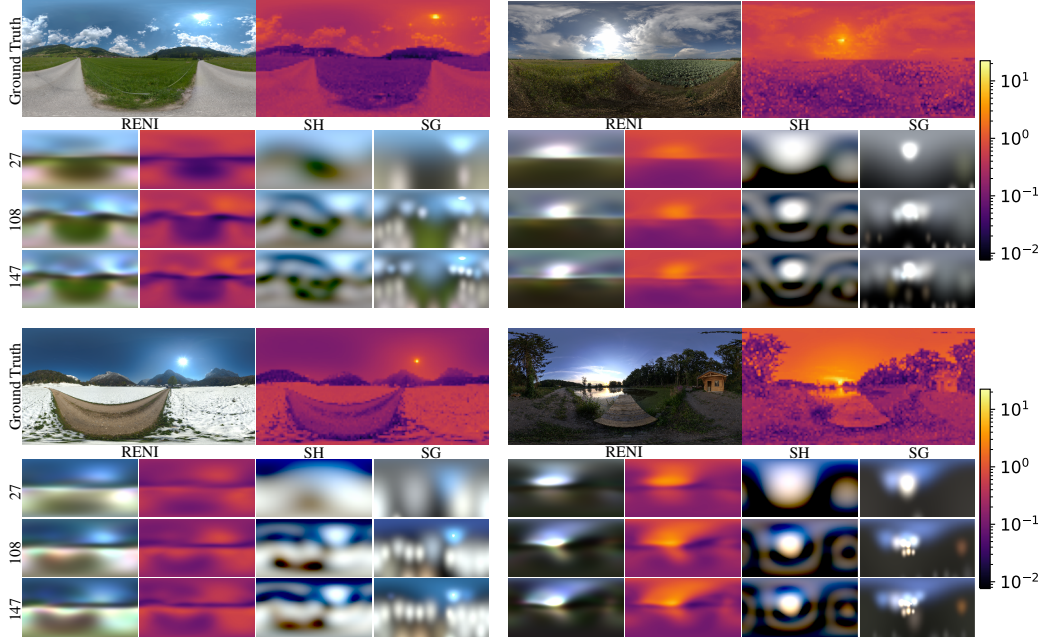


Figure 1: Generalisation to unseen images with latent code dimensions, $D = 3N$ for $N = 9, 36, 49$ and for SH of equal dimensionality (orders 2, 5, and 6). SG results are with dimensionality $D = 30, 108, 150$. Heat maps with log-scale colour bars for ground truth and RENI are also shown.



Figure 2: Generalisation to unseen images with latent code dimensions, $D = 3N$ for $N = 9, 36, 49$ and for SH of equal dimensionality (orders 2, 5, and 6). SG results are with dimensionality $D = 30, 108, 150$. Heat maps with log-scale colour bars for ground truth and RENI are also shown.



Figure 3: Fitting RENI and SH of latent dimension $D = 108$ to masked ground truth images. RENI realistically completes the environment whilst SH produces noisy, unrealistic results and overfits to the training data.

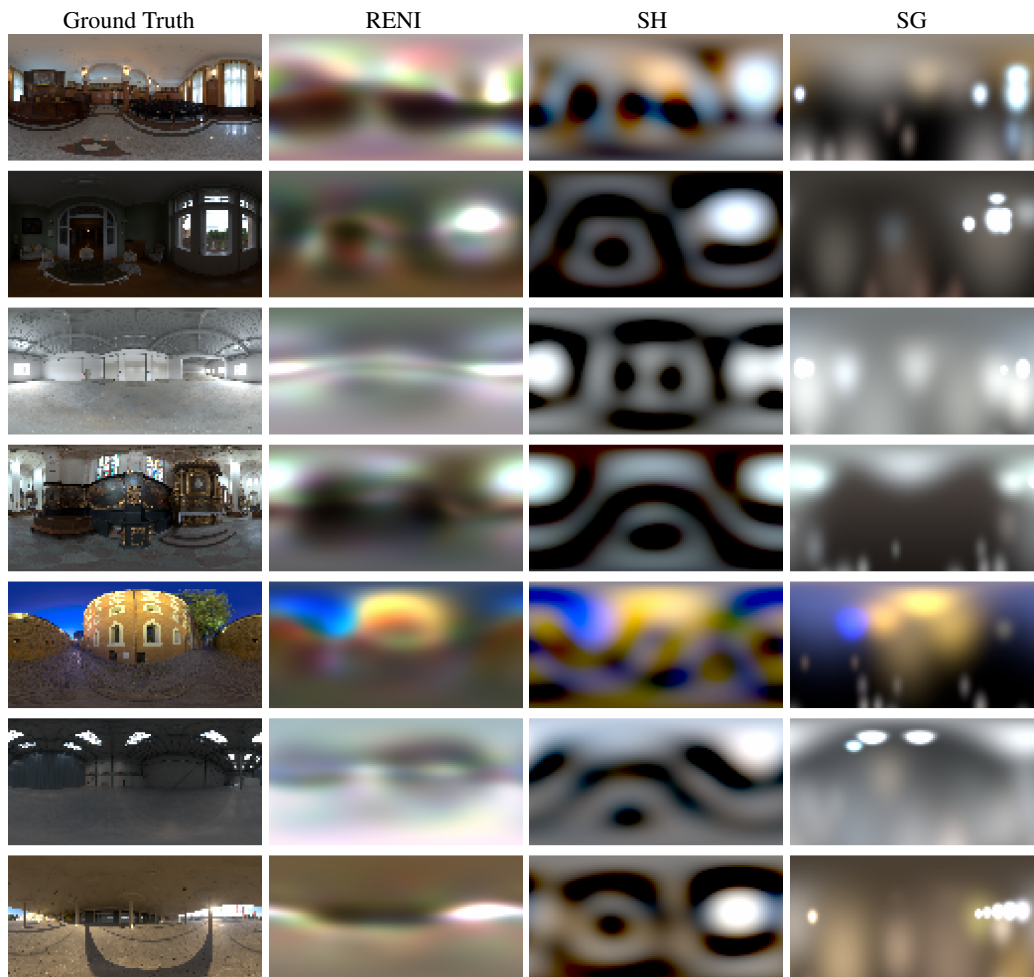


Figure 4: Fitting to images containing unnatural illumination conditions. Whilst these images are out-of-distribution for RENI, its latent space is expressive enough to still reasonably approximate some of these environments. RENI, SH and SG fit using models with $D = 108$.

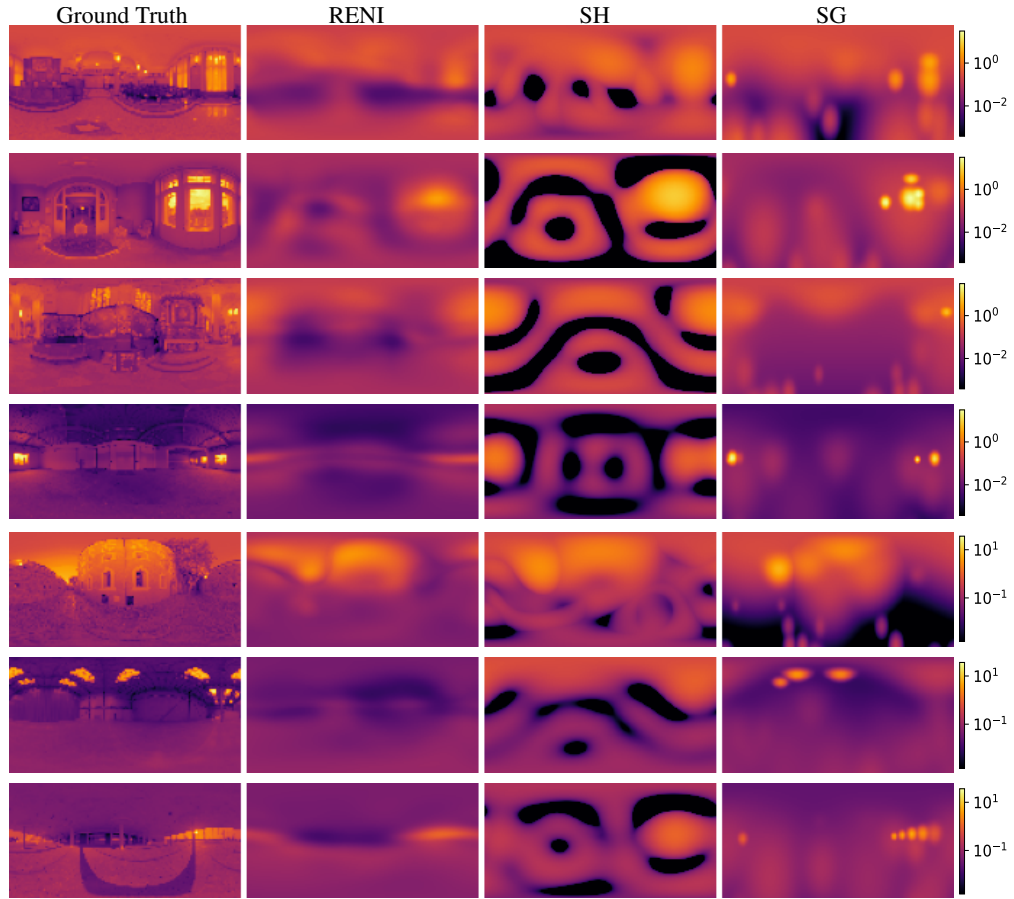


Figure 5: Heat maps with log-scale colour bars for images containing unnatural illuminations. RENI, SH and SG fit using models with $D = 108$.

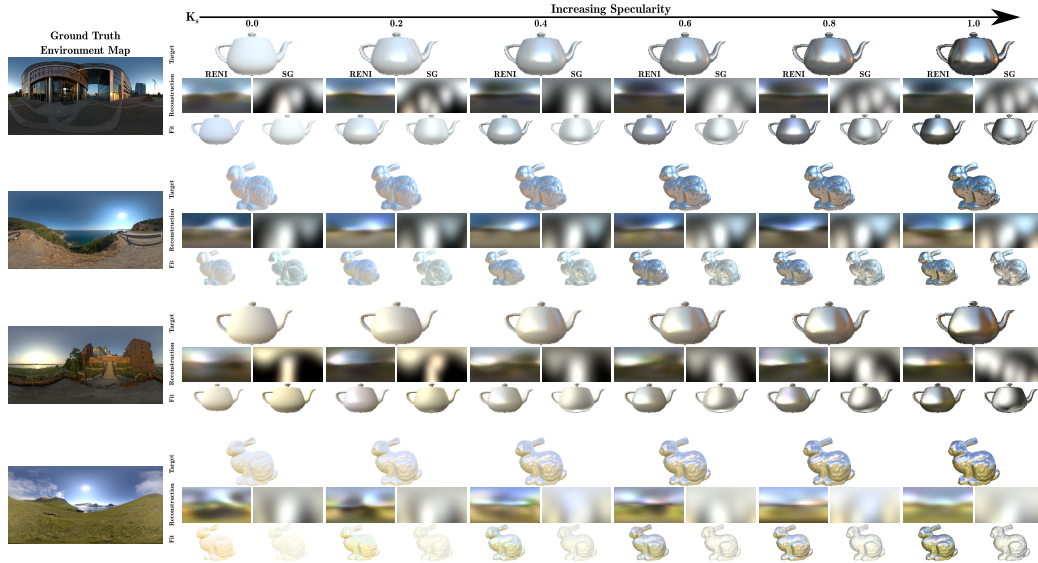


Figure 6: Reconstruction results in an inverse rendering task. The specular Blinn-Phong term K_s increases from left to right in steps of 0.2. RENI has a dimensionality of $D = 27$ and SG a dimensionality of $D = 30$. RENI outperforms SG whilst also producing environment maps that are plausible natural illumination environments as opposed to SG which produces arbitrary illuminations.



Figure 7: A failure case when interpolating between two training images using the $D = 108$ model. A reddish colour appears on the ground in the centre image that is not present in either the source or target images. This may be due to our use of HDR images. The source and particularly target have very bright sun regions; even though our loss is in log space, this likely dominates the reconstruction meaning slight colour tone errors in the darker regions are not penalised. Including the cosine loss function during training might help resolve this.